Water Research 194 (2021) 116928

Contents lists available at ScienceDirect

Water Research

journal homepage: www.elsevier.com/locate/watres

Simultaneous nitrate and sulfate dependent anaerobic oxidation of methane linking carbon, nitrogen and sulfur cycles

Wen-Bo Nie[a], Jie Ding[a], Guo-Jun Xie[a,*], Xin Tan[a], Yang Lu[b], Lai Peng[c], Bing-Feng Liu[a], De-Feng Xing[a], Zhiguo Yuan[d], Nanqi Ren[a]

[a] State Key Laboratory of Urban Water Resource and Environment, School of Environment, Harbin Institute of Technology, No.73, Huanghe Road, Nangang District, Harbin, Heilongjiang, 150090, China
[b] Singapore Centre for Environmental Life Sciences Engineering (SCELSE), Nanyang Technological University, Singapore 637551, Singapore
[c] School of Resources and Environmental Engineering, Wuhan University of Technology, 122 Luoshi Road, Wuhan 430070, China
[d] Advanced Water Management Centre, The University of Queensland, St Lucia, Brisbane QLD, 4072, Australia

ARTICLE INFO

Article history:
Received 25 September 2020
Revised 2 February 2021
Accepted 11 February 2021
Available online 13 February 2021

Keywords:
Sulfate-dependent anaerobic oxidation of methane
Nitrate-dependent anaerobic oxidation of methane
Dissimilatory nitrate reduction to ammonium
Nanonets
ANME-2d

ABSTRACT

ANaerobic MEthanotrophic (ANME) archaea are critical microorganisms mitigating methane emission from anoxic zones. In previous studies, sulfate-dependent anaerobic oxidation of methane (AOM) and nitrate-dependent AOM, performed by different clades of ANME archaea, were detected in marine sediments and freshwater environments, respectively. This study shows that simultaneous sulfate- and nitrate-dependent AOM can be mediated by a clade of ANME archaea, which may occur in estuaries and coastal zones, at the interface of marine and freshwater environments enriched with sulfate and nitrate. Long-term (~1,200 days) performance data of a bioreactor, metagenomic analysis and batch experiments demonstrated that ANME-2d not only conducted AOM coupled to reduction of nitrate to nitrite, but also coupled to the conversion of sulfate to sulfide, in collaboration with sulfate-reducing bacteria (SRB). Sulfide was oxidized back to sulfate by sulfide-oxidizing autotrophic denitrifiers with nitrate or nitrite as electron acceptors, in turn alleviating sulfide accumulation. In addition, dissimilatory nitrate reduction to ammonium performed by ANME-2d was detected, providing substrates to Anammox. Metatranscriptomic analysis revealed significant upregulation of *flaB* in ANME-2d and *pilA* in *Desulfococcus*, which likely resulted in the formation of unique nanonets connecting cells and expanding within the biofilm, and putatively providing structural links between ANME-2d and SRB for electron transfer. Simultaneous nitrate- and sulfate-dependent AOM as observed in this study could be an important link between the carbon, nitrogen and sulfur cycles in natural environments, such as nearshore environments.

1. Introduction

Methane (CH_4) represents an extremely potent greenhouse gas, with 28-fold higher potential than CO_2 to trap heat radiation on a molar basis in a 100-year time horizon (Pachauri et al., 2014), contributing about 20% of global warming potential (Fletcher and Schaefer, 2019). Anaerobic oxidation of methane (AOM) is a critical process mitigating methane emission from anoxic zones in marine and freshwater environments. As sulfate is a major terminal electron acceptor in ocean (about 28 mM), sulfate-dependent AOM is the dominant process for methane removal (Scheller et al., 2016), which consumes almost all methane (>90%) produced from marine sediments (Knittel and Boetius, 2009). Nitrate is prevalent in freshwater environments, especially in areas receiving agricultural runoff or untreated sewage (Deutzmann, 2020). Nitrate-dependent AOM was identified recently (Haroon et al., 2013) and demonstrated as a significant reduction for methane emissions that came from paddy fields (Vaksmaa et al., 2017b), wetlands (Shen et al., 2017) and riverbeds (Shen et al., 2019).

Sulfate-dependent AOM is performed by anaerobic methanotrophic archaea (ANME-1, ANME-2a/b/c and ANME-3) in syntrophy with sulfate-reducing bacteria (SRB) in marine system (Cassarini et al., 2018; Michaelis et al., 2002; Orphan et al., 2001b). Frequently, ANME-1 exist as rod-shaped single cells or in chains (Lloyd et al., 2011), without or only loosely forming associations with their SRB partners (Orphan et al., 2002). In contrast, ANME-2a/b/c and ANME-3 exist with SRB forming highly tight aggregates (Boetius et al., 2000; Holler et al., 2011; Knittel and Boetius 2009; Wang et al., 2014). These ANME archaea oxidize methane via the reverse methanogenesis and transfer reducing equivalents

* Corresponding author.
E-mail address: xgj@hit.edu.cn (G.-J. Xie).

https://doi.org/10.1016/j.watres.2021.116928
0043-1354/

to SRB with sulfate as the terminal electron acceptor (Eq. (1)) (Timmers et al., 2017). The direct interspecies electron transfer from ANME archaea to SRB was revealed through single cell activity mapping and metabolic modeling, which excluded diffusive intermediates as electron carriers (McGlynn et al., 2015). The nanowire-like structures were found to connect the ANME archaea and SRB cells, which further support direct interspecies electron transfer (Wegener et al., 2015). However, members of the ANME-2 clade were suggested to perform incomplete dissimilatory sulfate reduction to zero-valent sulfur via an yet unknow pathway (Milucka et al., 2012). Thus, the mechanism of sulfate-dependent AOM induced by ANME archaea is still under debate (Bhattarai et al., 2019).

$$CH_4 + SO_4^{2-} + 2H^+ \rightarrow CO_2 + H_2S_{(aq.)} + 2H_2O\ \Delta G^{\circ\prime} = -21\ kJ\ mol^{-1} \quad (1)$$

Distinct from marine system, nitrate-dependent AOM is carried out by a distinct ANME lineage, affiliated with a subgroup of ANME-2d and named *Candidatus* Methanoperedens nitroreducens, in freshwater environments (Eq. (2)) (Haroon et al., 2013; Shen et al., 2019). The clade of ANME-2d independently oxidizes methane in reverse methanogenesis providing electrons for nitrate reduction to nitrite (Arshad et al., 2015; Haroon et al., 2013), which could survive without bacterial partners, but require nitrite scavengers such as *Candidatus* Methylomirabilis oxyfera of NC10 phylum bacteria to avoid accumulation of toxic nitrite during nitrate-dependent AOM process (Hu et al., 2009; Raghoebarsing et al., 2006). ANME-2d clade also has the potential to couple AOM to dissimilatory nitrate reduction to ammonium (DNRA) (Ettwig et al., 2016; Gambelli et al., 2018), which could fuel Anammox bacteria in a biofilm reactor only fed with methane and nitrate (Nie et al., 2021). In addition, Fe (III)/Mn (IV) reduction (Ettwig et al., 2016) and humic substances reduction (Bai et al., 2019) associated with AOM by ANME-2d clade were observed. What's more, the clade of ANME-2d was previously related to sulfate-dependent AOM in lake sediments where nitrate was inadequate (Schubert et al., 2011; Su et al., 2019). However, the involvement of other electron acceptors (Fe (III)/Mn (IV)) for AOM process couldn't be excluded. Although the direct coupling of sulfate reduction with AOM driven by ANME-2d clade was speculated (Ino et al., 2018), the absence of genes for dissimilatory sulfate reduction suggested that ANME-2d could not support sulfate reduction by itself but with syntrophy mechanisms (Leu-et al. 2020b, Yu et al., 2018).

$$CH_4 + 4NO_3^- \rightarrow CO_2 + 4NO_2^- + 2H_2O\ \Delta G^{\circ\prime} = -521\ kJ\ mol^{-1} \quad (2)$$

Estuary or coastal zones not only receive reactive nitrogen compounds (e.g. nitrate discharged from agriculture land) but also suffer from intrusion of seawater (Ferguson and Gleeson 2012). In addition, sulfate concentration in freshwater environments continuously increases due to the use of agricultural fertilizers containing sulfate (Szynkiewicz et al., 2011), anthropogenic sulfate input from industries (e.g. food processing, pharmaceutical, paper processing and mining activities) (Khanal and Huang 2003) and atmospheric sulfur deposits (Clark et al., 2019). As a result, nitrate and sulfate would be major terminal electron acceptors in nearshore sediments (Laverman et al., 2012) and some freshwater environments (Chen et al., 2016; Lamers et al., 1998), which offers important habitats for microorganisms involved in the carbon, nitrogen and sulfur cycles. However, the link of nitrogen and sulfur cycles by simultaneous nitrate- and sulfate-dependent AOM is still unknown. Given the coexistence of methane, sulfate and nitrate in nearshore sediments, a methane-based membrane biofilm reactor fed with nitrate and sulfate was operated for 1200 days to mimic the subsistence of microbial communities in natural sediments (Chadwick et al., 2019). Performance of the reactor was closely monitored, and the dynamics of microbial community was investigated through 16S rRNA gene amplicon sequencing. Transformations of methane, nitrate and sulfate were determined through batch tests and microelectrode analysis of biofilm. The microstructure of biofilm was revealed by scanning electron microscope (SEM) to identify structural link between ANME-2d and their bacterial partners. Simultaneous nitrate- and sulfate-dependent AOM driven by ANME-2d were also verified through metagenomic and metatranscriptomic analyses.

2. Materials and methods

2.1. Bioreactor configuration and operation

A lab-scale membrane biofilm reactor (MBfR) with a work volume of 645 mL was equipped with 8 bundles of gas-permeable hollow fiber membranes (OxyMem, Ireland) for continuous supply of methane (v/v: 95% CH_4 /5% CO_2), and a water jacket was used for temperature control (Fig. S1 and SI Text A). The phases of the MBfR operation are summarized in Table 1. Initially, the reactor was inoculated with 100 mL sludge from a parent bioreactor where ANME-2d archaea, NC10 bacteria and Anammox bacteria were dominant (Nie et al., 2019). After inoculation, concentrated nitrate and sulfate solution was daily pulse-dosed into the reactor to maintain the bulk nitrate and sulfate concentration in the range of 20~50 mg N/S L^{-1} for biofilm development (Phase I). From Day 104, the reactor was turned into continuous operation (Phase II~VIII). The influent contained nitrate and sulfate (Table 1), as well as mineral medium for microbial growth (SI Text B). The hydraulic retention time (HRT) was initially set at 2.1 days and then stepwise decreased due to the constantly low concentrations of nitrate in effluent (Table S1). After stable operation at 30 °C, the temperature was decreased to 25 °C on Day 506 (Phase III), then progressively reduced at interval of 1 °C to 10 °C (Phase IV) and to 5 °C (Phase V). Finally, the temperature of the MBfR operation was held constant at 5 °C from Day 1109 (Phase VI-VIII), which is close to temperature in nature sediments (Biddle et al., 2012; Gudasz et al., 2010). The more specific parameters of the reactor operation are listed in Supplementary Information (Table S1).

2.2. Batch tests in MBFR

In order to confirm the active bio-reaction and electron balance of the simultaneous nitrate- and sulfate-dependent AOM in the biofilm, Batch tests were undertaken at the end of Phase V. The conditions of each batch test are summarized in Table 2. The methane consumption rate was calculated based on the nitrate and sulfate consumption rate, nitrite, ammonium and sulfide production rate, and the microbial community (as described in SI Text C).

To measure the methane consumption, the MBfR was disconnected from the methane gas cylinder to terminate methane supplying. The bulk liquids in MBfR were replaced by freshly prepared medium. The prepared medium was sparged with the gas mixture (95% CH_4 and 5% CO_2) for 10 min at a flow rate of 500 mL min^{-1}, which made the medium rich in dissolved methane. The liquid phase in the MBfR was continuously circulated during the batch tests. The three batch tests were run in the batch mode for 12 h, with liquid samples collected at hourly intervals. At the end of each batch test, the biofilm samples were collected to determine the transcription levels of gene *mcrA* associated with the reverse methanogenic pathway; gene *narG* associated with nitrate reduction pathway; gene *dsrA* associated with dissimilatory sulfate reduction pathway and genes *cytC*, *flaB* and *pilA* associated with extracellular electron transfer.

Table 1
Operational conditions of the MBfR during long-term experiment.

Phase	Operation time	Influent composition (mg N/S L^{-1})		Temperature (°C)	Comments
		NO_3^-	SO_4^{2-}		
I	Day 0~103	NA[a]	NA[a]	30	Start-up phase of the reactor
II	Day 104~505	50.5 (±0.9)	40.3 (±0.6)	30	Stepwise reduction of HRT[b] to increase nitrate and sulfate loading rate
III	Day 506~545	51.2 (±0.4)	41.0 (±0.7)	25	Operated at 25 °C
IV	Day 546~913	50.8 (±0.7)	40.5 (±0.3)	from 25 to 10	Stepwise reduction of temperature from 25 to 10 °C
V	Day 914~1,108	52.9 (±1.5)	40.7 (±0.4)	from 10 to 5	Stepwise reduction of temperature from 10 to 5 °C
VI	Day 1,109~1,127	51.4 (±0.9)	80.9 (±1.1)	5	Increase of the sulfate concentration in influent
VII	Day 1,128~1,145	35.2 (±0.3)	81.1 (±0.8)	5	Decrease of the nitrate concentration in influent
VIII	Day 1,146~1,200	20.7 (±0.6)	160.3 (±0.8)	5	Decrease of the nitrate concentration and increase of the sulfate concentration in influent

[a] : not available, the MBfR was operated in batch during the start-up phase;
[b] : hydraulic retention time.

Table 2
Rates of anaerobic methane oxidation when fed with different substrates in Batch Test A-I, A-II and A-III.

Batch No.	Feeding (mM)			Measured rate (mM d^{-1})[a]					Predicted rate (mM d^{-1})[b]	Comments
	NO_3^-	SO_4^{2-}	CH_4	rNO_3^-	rNH_4^+	rNO_2^-	rS^{2-}	rCH_4	rCH_4	
Batch Test A-I	3.45	0	1.21	-3.82	0.29	1.28	NA[c]	-1.97	-2.02 (-2.54%)[d]	Nitrate-dependent anaerobic methane oxidation
Batch Test A-II	0	1.46	1.14	NA	NA	NA	2.43	-2.36	-2.43 (-2.97%)	Sulfate-dependent anaerobic methane oxidation
Batch Test A-III	3.51	1.47	1.13 (1.20)[e]	-5.73	0.01	0.01	0.55	-4.19	-4.13 (1.43%)	Simultaneous nitrate- and sulfate-dependent anaerobic methane oxidation

[a] : the nitrate, ammonium, nitrite, sulfide and methane conversion rates calculated by linear regression of their respective concentration profiles;.
[b] : the methane predicted conversion rate based on the hypothesized reactions match well with the measured conversion rate;.
[c] : not available;.
[d] : the values in bracket are balancing errors: (measured value – predicted value)/ measured value *100%;.
[e] : the concentration of dissolved methane was replenished at 6 h.

2.3. cDNA synthesis and RT-qPCR

The transcription levels of genes *mcrA, narG, dsrA, pilA, flaB* and *cytC* in batch tests were quantitatively measured by the reverse transcriptase quantitative polymerase chain reaction (RT-qPCR). cDNA synthesis was conducted by PrimeScript RT-PCR kit (Perfect Real Time) and gDNA Eraser (TaKaRa, China), according to manufacturer's protocol. RT-qPCR was accomplished by an ABI 7500 system (Applied Biosystems, China) with SYBR Premix Ex *Taq* (TaKaRa, China) using published primers (Table S2). The transcription levels of each functional gene were normalized against the total 16S rRNA gene copies since 16S rRNA gene copies were relatively stable during the batch tests (Kapoor et al., 2015). The detailed methods of RT-qPCR were referred to the previous study (Nie et al., 2021).

2.4. Microelectrode measurements

For the measurement of substrate profiles in the biofilm, biofilms in the reactor were cultured for 6 h with the influent containing nitrate only, sulfate only, nitrate and sulfate, respectively. Concentration gradients of NO_3^-, NO_2^-, NH_4^+, SO_4^{2-} and S^{2-} within biofilm were measured with a suite of microelectrodes. Liquid ion-exchange (LIX) membrane microsensors with tip diameters of approximately 10~15 μm for NO_3^--N, NO_2^--N and NH_4^+-N measurements were prepared according to a previous description (deBeer et al., 1997). The microelectrode for measurement SO_4^{2-} and S^{2-} in biofilm with a tip diameter of about 20 micrometers was used and operated referring to a previous description (Liu et al., 2020). The microelectrode placed inside a faraday cage was mounted on a motor-driven micromanipulator (MM33–2, Unisense, Denmark). Each measurement of different positions along the biofilm axis was performed three times by advancing the microelectrode at depth steps of 50 μm through the biofilm.

2.5. Fluorescence in situ hybridization

Biofilm samples were taken from the reactor on Day 1200, and fixed by a PBS-buffered (pH=7.2) 4% (v/v) paraformaldehyde (Sigma, Germany) solution for 45 min at room temperature (Glöckner et al., 1996). Hybridization was performed using 40% formamide as described in previous work (Ettwig et al., 2008). The oligonucleotide probes (Table S3) were purchased with specific fluorescence labels from Sangon Biotech Co., Ltd. (Shanghai, China). Hybridized slides were examined via a Zeiss (LSM800) confocal laser scanning microscope (Carl Zeiss Meditec AG, Jena, Germany).

2.6. Sample processing and SEM analysis

At the end of operation (Day 1200), biofilm samples were collected and first fixed with 2.5% glutaraldehyde in phosphate buffer (0.1 M, pH = 7.0) for over 4 h and then washed three times in the phosphate buffer for 15 min at each step. Post fixation and dehydration of biofilm samples were then carried out (SI Text D). The dehydrated sample was coated with gold palladium in a Hitachi Model E-1010 ion sputter for approximately 5 min and observed in a Hitachi SU8010 SEM for morphological analysis.

2.7. Chemical analytical methods

Liquid samples were immediately filtered through Millipore filter units (0.22-μm pore size) for the analysis of NO_3^--N, NO_2^--N, NH_4^+-N,.SO_4^{2-}-S and S^{2-}-S. The concentrations of NO_3^--N, NO_2^--N, NH_4^+-N and SO_4^{2-}-S were measured with a Lachat QuikChem8500 Flow Injection Analyzer (Lachat Instrument, Milwaukee, WI) (Jiang et al., 2009; Pasquali et al., 2007). The concentration of S^{2-}-S was measured immediately using the methylene blue method (Miner, 2006). An Agilent 7890A (Agilent, USA) gas chromatograph equipped with an electron capture detector (ECD) was used to measure dissolved methane concentrations.

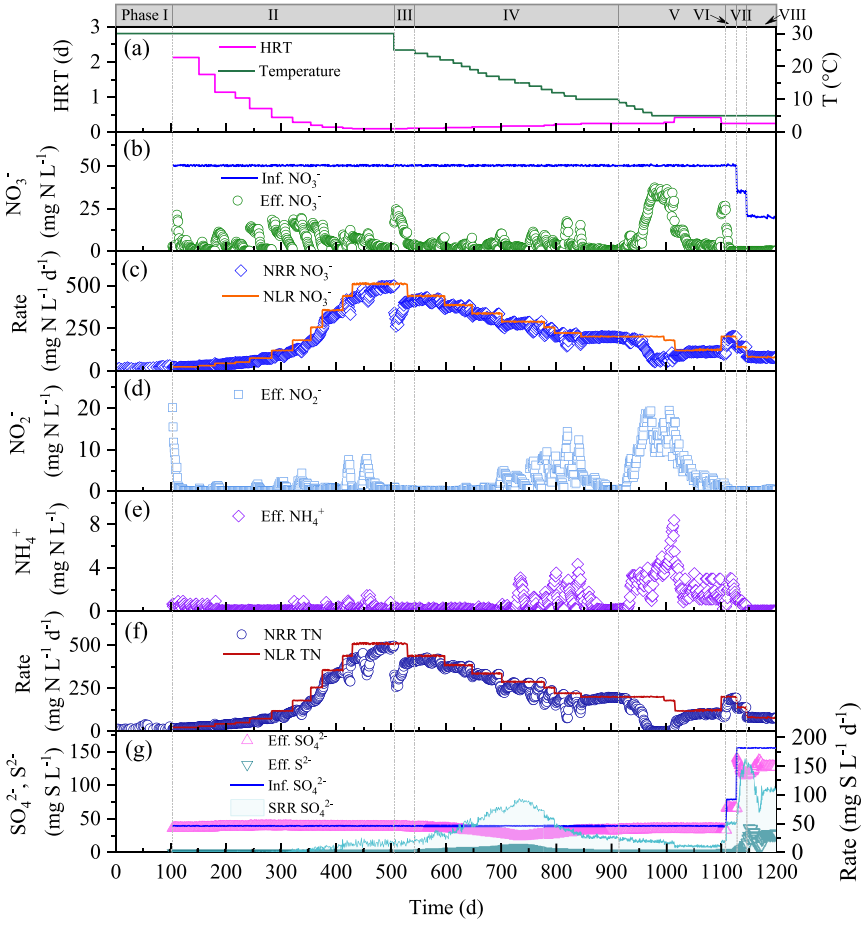

Fig. 1. Reactor performance during long-term operation of MBfR. (a) the HRT and temperature for MBfR operation; (b) variation of NO_3^- concentration in influent and effluent; (c) NO_3^- loading rate and NO_3^- removal rate; (d) variation of NO_2^- concentration in effluent; (e) variation of NH_4^+ concentration in effluent; (f) total nitrogen loading rate and total nitrogen removal rate; (g) variations of SO_4^{2-} concentration in influent, SO_4^{2-} and S^{2-} concentrations in effluent, and SO_4^{2-} removal rate. Phase I for reactor start-up: Day 0~103; Phase II-VIII for reactor continuous operation: Day 104~1200. HRT: hydraulic retention time; Inf.: influent; Eff.: effluent; NRR: nitrogen removal rate; NLR: nitrogen loading rate; TN: total nitrogen; SRR: sulfur removal rate.

2.8. DNA and RNA library preparation and sequencing

Twelve biofilm samples were collected from the biofilm sampling port of the reactor on Day 0, 103, 250, 456, 540, 640, 750, 835, 910, 970, 1080 and 1175 for biological analysis. Each biofilm sample was divided equally into two parts for DNA and RNA extraction, which were centrifuged at 4 °C with 10,000 × g for 15 min by a high-speed centrifuge (HERMLE Labortechnik GmbH, Germany) for obtaining cell pellets. The DNA of biofilm samples was extracted using the FastDNA spin kit for soil (MO-BIO Laboratories Inc.) following the manufacturer's instructions. A part of the DNA was analysed with 16S rRNA gene amplicon sequencing, and the other part was analysed with metagenomic sequencing. Another biofilm sample was frozen with liquid nitrogen and preserved in 1 mL of RNAlater (Ambion) at -80 °C until nucleic acid extraction. The RNA of biofilm samples was extracted using TRIzol reagent (Invitrogen, USA) according to manufacturer's protocol, and purified by RNA clean kit (Tiangen, China). Primers 926_F and 1392_R targeting the V6–8 region of 16S rRNA gene were used for PCR (Engelbrektson et al., 2010).The detailed methods of PCR amplification, 16S rRNA amplicon sequencing, and metagenomic and metatranscriptomic sequencing are described in Supplementary Information (SI Text E). Sequencing data are deposited on the NCBI Short Read Archive under accessions numbers of SAMN15394707-SAMN15394709 and SAMN15398743-SAMN15398745.

2.9. Metagenomic assembly and binning

All of raw reads from the constructed libraries generated by Illumina HiSeq sequencers were quality trimmed by homemade Perl scripts (Hua et al., 2015), and the trimmed sequences were filtered with Sickle version 1.33 based on the parameters of "-q 20 -l 50″ (Joshi and Sickle, 2011). Then, contigs and scaffolds were assembled by SPAdes version 3.11.0 with default parameters (Bankevich et al., 2012). As a sequence pool, all high-quality reads were mapped on them by BBMap version 38.85 with the parameters of "k = 15 minid=0.97 build=1″. These scaffolds generated were binned into the draft genomes by MetaBAT version 0.32.5 with the sensitive model, which considers abundance and tetranucleotide frequency (Kang et al., 2015). The recovered draft genomes were assessed for genome completeness and potential contamination by CheckM version 1.0.7 (Parks et al., 2015). The genome bins with completeness of >50% were kept and then optimized for removing the contaminations.

2.10. Analyses of genome bins

The functional annotations for each bin were curated and revised based on the comparison with the databases to the KEGG, eggnog and NCBI-nr by the Diamond programs with the blast e value of $1e^{-5}$ (Buchfink et al., 2015). Based on the gene annotations, all the predicted putative genes were mapped onto different

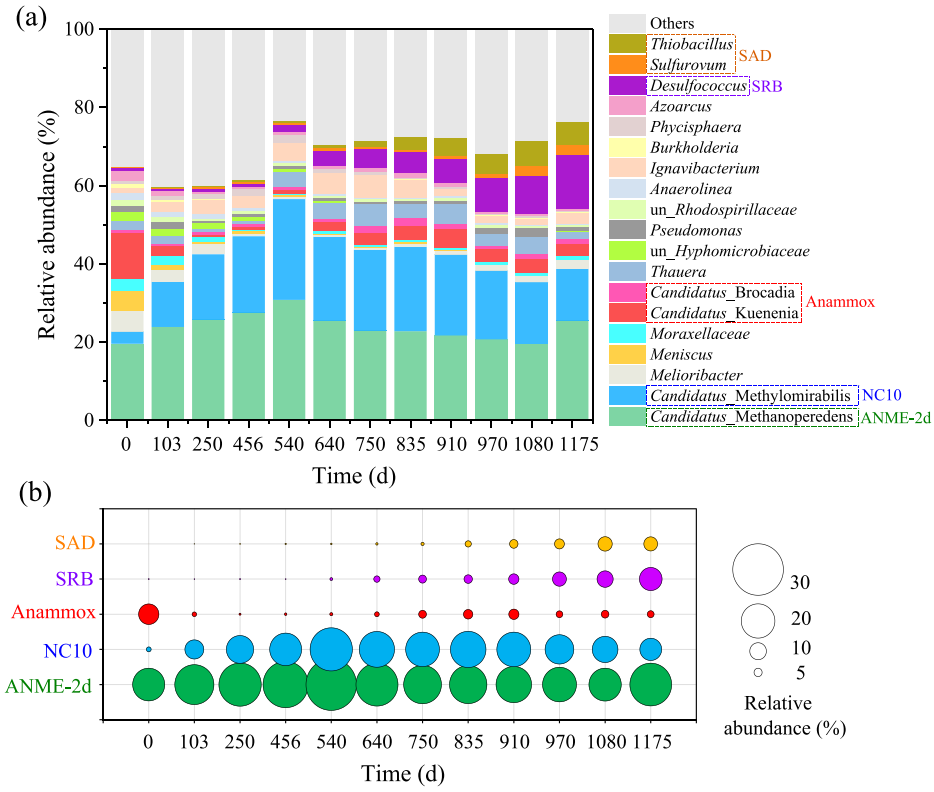

Fig. 2. Microbial community dynamics of the biofilm during long-term operation of MBfR fed with methane, nitrate and sulfate. (a) relative genus-level abundance of microbial population and (b) relative abundance of the key microbes, including sulfide-oxidizing autotrophic denitrifier (SAD) (*Thiobacillus* and *Sulfurovum* spp.), sulfate-reducing bacteria (SRB) (*Desulfococcus* spp.), Anammox bacteria (*Candidatus* Kuenenia and *Candidatus* Brocadia spp.), NC10 bacteria (*Candidatus* Methylomirabilis spp.) and ANME-2d archaea (*Candidatus* Methanoperedens spp.). Genera with an abundance of >0.1% in at least one sample are presented. The abundance values are shown in Table S5.

modules in KEGG system using KAAS (Moriya et al., 2007), especially onto relevant methane, nitrogen, sulfur, flagellar and pilus metabolism. The 16S rRNA gene sequences were identified with RNAmmer (Lagesen et al., 2007) and the closely related 16S rRNA gene sequences in NCBI Gen-Bank were searched with BLASTN (Buhler et al., 2007). The calculation methods of relative abundance and transcript abundance for expression level of each gene were as reported previously (Tan et al., 2019) (further described in SI Text F). One-way analysis of variance (*ANOVA*) by SPSS 16.0 was used to determine the gene expression differences between samples in each bin.

3. Results

3.1. Reactor performance and microbial community dynamics

The performance of the methane-based MBfR for biotransformation of nitrogen and sulfur during the whole operation is shown in Fig. 1. The average methane oxidation rate at a steady state during each phase was calculated and shown in Table S4.

After inoculation, an increase in nitrate removal rate from about 10 to 30 mg NO_3^--N L^{-1} d^{-1} was observed during phase I for the MBfR startup (Day 0~103) (Fig. 1c). At a steady state of phase I, total NRR was stable at about 25 mg N L^{-1} d^{-1} (Fig. 1f). During phase II, nitrate accumulated obviously in effluent with the decreased HRT, then gradually declined to below 1 mg NO_3^--N L^{-1} d^{-1} (Fig. 1b). Afterwards, the HRT was stepwise shortened to 0.1 days on Day 430 (Fig. 1a), resulting in an increased nitrate removal rate and total NRR to 500 and 497 mg N L^{-1} d^{-1}, respectively (Day 505) (Fig. 1c and f). From phase III to phase V, the performance of nitrogen removal was restricted by the stepwise decrease of operational temperature (Fig. 1a, c and f). The nitrate conversion rate dropped to about 110 mg NO_3^- L^{-1} d^{-1} at 5 °C (Fig. 1c). During those periods, there was not only significant accumulation of nitrate in effluent, but also accumulation of nitrite and ammonium (Fig. 1b, d and e), which resulted in the total NRR at the steady state of only about 95 mg N L^{-1} d^{-1} (Fig. 1f).

The concentration of sulfate in effluent started to decrease from around Day 350 (phase II), accompanied by an increase of effluent sulfide, with a sulfate removal rate of about 90 mg S L^{-1} d^{-1} achieved by Day 748 (Phase IV) (Fig. 1g). Sulfate removal rate then gradually decreased and was stabilized at about 10 mg S L^{-1} d^{-1} at the steady state of phase V, without accumulation of sulfide in effluent (Fig. 1g). When the sulfate concentration in influent was increased from 40 to 80 mg SO_4^{2-}-S L^{-1} during phase VI, the sulfate removal rate increased to about 50 mg S L^{-1} d^{-1} (Fig. 1g). Interestingly, higher sulfate reduction rate produced more sulfide, that provided more electron donors for nitrate reduction, resulting in the nitrate removal rate increased to 200 mg N L^{-1} d^{-1} in this period (phase VI) (Fig. 1c). What's more, the increase of sulfate in influent also enhanced the rate of AOM (Table S4). When nitrate in influent decreased, there was significant accumulation of sulfide in effluent (Fig. 1b and g), and the decrease in the rate of AOM was evident (Table S4).

Analysis of 16S rRNA gene amplicon sequences confirmed that genera *Ca.* Methanoperedens, *Desulfococcus, Ca.* Methylomirabilis, *Thiobacillus, Sulfurovum, Ca.* Kuenenia and *Ca.* Brocadia dominated in the biofilm at the end of reactor operation with relative abundance of 25.5%, 13.8%, 13.4%, 6.1%, 2.4%, 2.9% and 1.4%, respectively (Fig. 2a and Table S5). All ANME archaea detected in biofilm fell within one genus *Ca.* Methanoperedens of ANME-2d clade

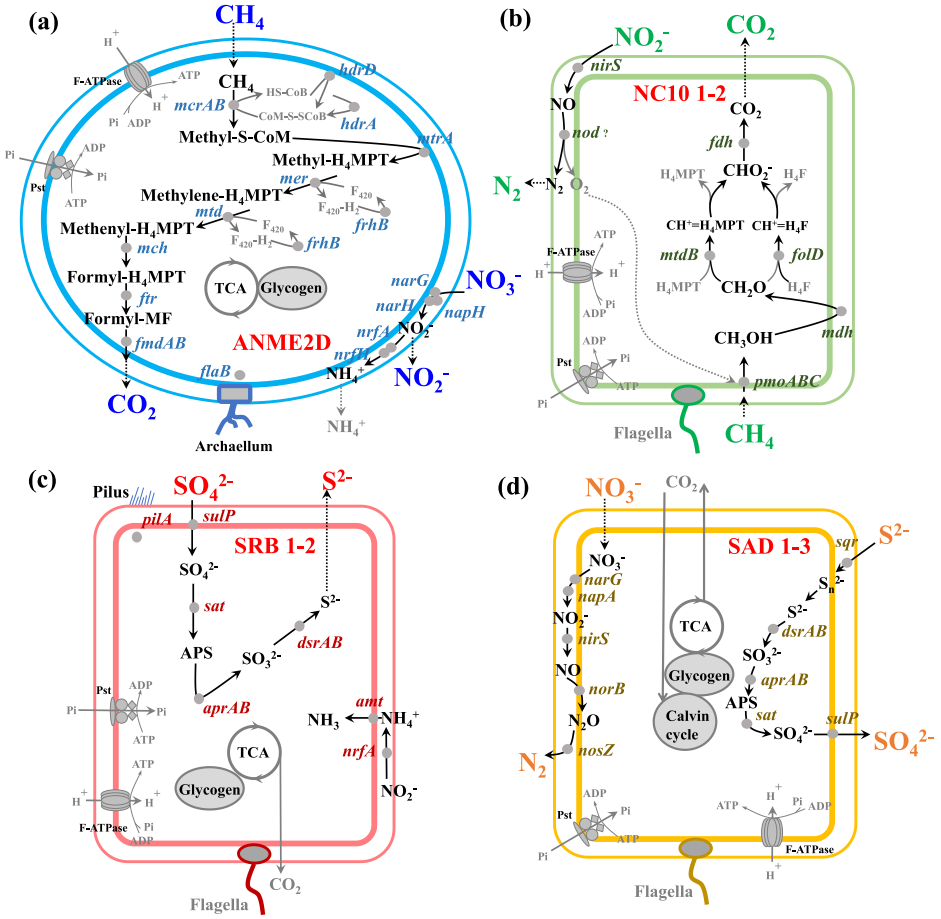

Fig. 3. The draft genomes assembled from metagenomic data of the key microbes in biofilm. (a) Draft genome ANME2D associated with *Candidatus* Methanoperedens nitroreducens; (b) draft genomes NC10 1and NC10 2 associated with *Candidatus* Methylomirabilis oxyfera; (c) draft genomes SRB 1 and SRB 2 asscociated with *Desulfococcus* and (d) SAD 1 associated with *Thiobacillus*, and SAD 2 and SAD 3 associated *Sulfurovum*. The pathways associated with methane, nitrogen and sulfur are shown.

(Fig. 2a, b and S2). Its relative abundance increased from 19.7% initially, to 30.8% on Day 540, and then stabilized at about 20% during Day 750~1080 (Fig. 2b). The *Desulfococcus* spp., a typical SRB cooperating with ANME archaea (Bhattarai et al., 2019), was detected in the inoculum with the relative abundance of only 0.7% and gradually increased to 13.8% on Day 1175. The genus *Thiobacillus* and *Sulfurovum*, with a known function of sulfide-oxidizing autotrophic denitrifier (SAD) (Liu et al., 2016a; Moraes et al., 2011), also had an increase in their relative percentage from 0.2% to 8.8% on Day 1080. The increased abundance of genus *Ca.* Methylomirabilis belonging to NC10 phylum from 3.0% to 25.8% on Day 540 was observed, but then it was decreased slightly (Fig. 2b). Due to the lack of ammonium in feed, the relative abundance of Anammox (*Ca.* Kuenenia and *Ca.* Brocadia spp.) decreased significantly from the initial 12.3% to 1.3% on Day 250 (Fig. 2b). However, Anammox re-emerged in the biofilm after Day 540. The accumulation of nitrite and ammonium in effluent could provide substrates for the growth of Anammox bacteria (Fig. 1d and e).

3.2. Metabolic pathways of the microbial populations

Metagenomic and metatranscriptomic sequencings were performed on biofilm samples collected on Day 0, 910 and 1175. The metagenomic data (Table S6) allowed assembly of 8 high-quality draft genomes, which ranged in size from 2.7 to 5.7 Mb and GC content from 43.4 to 66.5%. These included Bin ANME2D for *Ca.* Methanoperedens, Bins NC10 1–2 for *Ca.* Methylomirabilis, Bins SRB 1–2 for *Desulfococcus*, Bin SAD 1 for *Thiobacillus* and Bins SAD 2–3 for *Sulfurovum*. The main metabolic potentials of those microorganisms (Fig. 3a~d and Table S7) were constructed from the metagenomes, which were described in conjunction with gene expressions evaluated through metatranscriptomics (Table S8 and S9). The highest abundance (RPKM) and the highest relative transcriptional activity (RTA) of 20 transcripts as a whole were characterized, among which 13 transcripts involved in methane metabolism (map00680) (*mcrA, fmdA, frhB, mer, mtd* and *ftr*), nitrogen metabolism (map00910) (*narG, nirS, norB* and *nosZ*) and sulfur metabolism (map00920) (*dsrA, aprB* and *sulP*) were shared by both expression profiles of the RPKM and RTA (Fig. 4). The unshared expression transcripts were associated with methane metabolism genes *pmoAC, mdh, fdhB, folD, mch* and *fmdB*, nitrogen metabolism genes *nrfA* and *napA*, sulfur metabolism genes *aprA, dsrB* and *sat*, archaeal flagellin of gene *flaB*, and type IV pilus assembly protein of gene *pilA* (Fig. 4).

The expression of gene *narG* encoding nitrate reductase was mainly confirmed in Bin ANME2D and SAD 1–3, illustrating that nitrate removal in the MBfR was owing to both ANME-2d and SAD. The analysis of gene expression revealed that gene *narG* is highly expressed in both microbes. However, a significant disparity in RPKM values of the gene *narG* in SAD with time (*ANOVA*, $P \leq 0.05$) was observed. The nitrate reductase RTA in SAD as a whole increased significantly over time ($P \leq 0.05$) and in ANME-2d declined slightly after an initial increase, indicating that the nitrate removal function in the MBfR gradually shifted from solely by ANME-2d to jointly by ANME-2d and SAD. The expression of

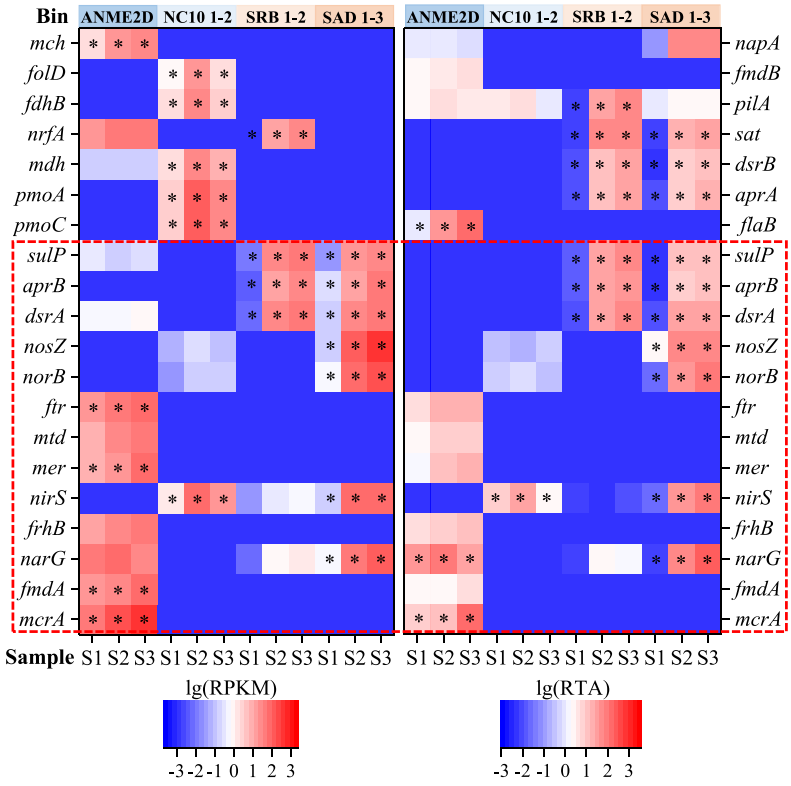

Fig. 4. The heat map represents the expression profiles for top 20 genes with relative abundance (RPKM) and relative transcriptional activity (RTA). S1, S2 and S3 represent the samples obtained on Day 0, 910 and 1175, respectively. Genes circled by red dashed rectangle were shared by both two expression profiles at RPKM and RTA levels. The black asterisks were given representing the gene transcript is significantly different comparing with that in other samples by using *ANOVA* analysis. The abbreviations for metabolites and definitions for genes have been listed in Table S8 and S9.

gene *nirS*, encoding nitrite reductase in NC10 bacteria, also had a trend of a gradual decrease following an initial rise, in both RPKM and RTA levels, while that in SAD increased with operation time. As in the case of nitrate reduction to nitrite, nitrite reduction was initially performed mainly by NC10 and then jointly by NC10 and SAD. The expressions of genes *norB* and *nosZ* possessed by SAD for the further reduction of nitric oxide and nitrous oxide supported the role of SAD in nitrite reduction (Fig. 4). The high expression of genes *sulP, aprB* and *dsrA* (as the shared top 20 transcripts in both RPKM and RTA) was observed in both Bins SRB 1–2 and SAD 1–3, which are required for sulfate dissimilatory reduction and sulfide oxidation. The significantly increased RTA of genes *sat, dsrB* and *aprA* over time was also present in both Bins SRB 1–2 and SAD 1–3 ($P \leq 0.05$).

The gene groups associated with the reverse methanogenic pathway, including genes *mcrA, fmdAB, frhB, mer, mtd, ftr* and *mch*, showed an overall increasing trend in both RPKM and RTA levels, while the gene groups (*pmoAC, mdh, fdhB* and *folD*) associated with the intra-aerobic methane oxidation pathway (using the oxygen produced intracellularly from dismutation of nitric oxide under anaerobic condition) showed significant downregulation after a temporary increasing trend. With the increased sulfate concentration and decreased nitrate concentration in the influent for the MBfR, there were significant up-regulation of expression of genes associated with reverse methanogenesis in ANME-2d and sulfate dissimilatory reduction in *Desulfococcus* but downregulation of *narG* expression for nitrate reduction in ANME-2d This provides evidence for the AOM by ANME-2d supporting sulfate reduction. Further, statistical analyses demonstrated that the RTA level of *flaB* and *pilA* in ANME-2d and *Desulfococcus*, respectively, increased significantly (both $P \leq 0.05$) during operation of MBfR (Fig. 4).

3.3. Biotransformation of methane, nitrogen and sulfur in biofilm

The nitrate, nitrite, ammonium, sulfate, sulfide and dissolved methane profiles measured in Batch Test A-I, A-II and A-III are shown in Fig. 5. With nitrate as electron acceptor in Batch Test A-I, the concentration of nitrate dropped from 3.45 to 1.51 mM within 12 h, accompanied by ammonium and nitrite accumulation of 0.18 and 0.66 mM, respectively (Fig. 5a). In contrast, when nitrate and sulfate co-existed as electron acceptors in Batch Test A-III, there was a higher nitrate removal rate of about 5.73 mM and almost no accumulation of ammonium and nitrite in the same incubation time (Table 2 and Fig. 5c). However, the rates of sulfate conversion and sulfide accumulation with sulfate as single electron acceptor in Batch Test A-II were higher than that in the case of nitrate and sulfate co-existence (Table 2 and Fig. 5b). As summarized in Table 2, the predicted dissolved methane consumption rate compares very well with the measured rate in all case, with mass balance errors below 5% (Table 2). The difference was that the AOM rate of 4.19 mM d^{-1} was highest under the condition of nitrate and sulfate co-existence as electron acceptors for AOM (Table 2). The expression patterns of key genes, related to reverse methanogenic pathway (*mcrA*), nitrate reduction pathway (*narG*), dissimilatory sulfate reduction pathway (*dsrA*), extracellular electron transfer (*cytC*) and formation of conductive appendages (*flaB* and *pilA*), in Batch Test A-I, A-II and A-III were further investigated, as shown in Fig. 5d. Comparing relative gene expression of ANME-2d in consortial growth using sulfate (or sulfate plus nitrate), versus single growth using nitrate, genes *cytC, pilA* and *flaB* were clearly overexpressed, this was also the case when compared to gene *dsrA* expression (Fig. 5d). In addition, the combination of nitrate and sulfate as electron acceptors caused a significant over-

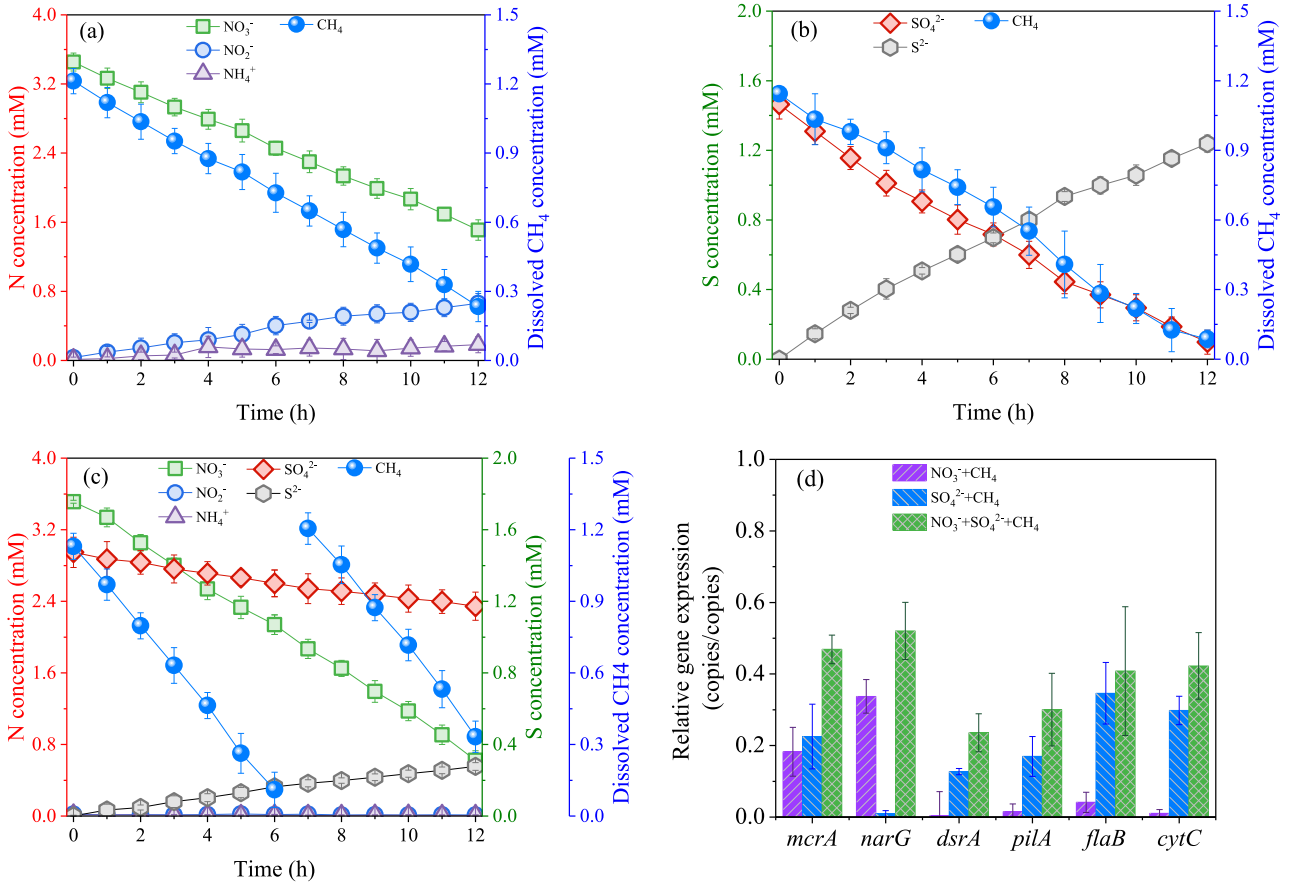

Fig. 5. Biotransformation of methane, nitrogen and sulfur in the MBfR. (a) nitrate-dependent AOM in the presence of nitrate and dissolved methane (initial nitrate concentration, 3.45 mM; initial dissolved methane concentration, 1.21 mM; 12-hour incubation); (b) sulfate-dependent AOM in the presence of sulfate and dissolved methane (initial sulfate concentration, 1.46 mM; initial dissolved methane concentration, 1.14 mM; 12-hour incubation); (c) simultaneous nitrate- and sulfate-dependent AOM in the presence of nitrate, sulfate and dissolved methane (initial nitrate concentration, 3.51 mM; initial sulfate concentration, 1.47 mM; initial dissolved methane concentration, 1.13 mM; 12-hour incubation; the concentration of dissolved methane was replenished at 6 h through overflow bottle of the MBfR system); (d) expression of genes *cytC, flaB, pilA, dsrA, narG* and *mcrA* in incubations with nitrate and methane (purple), sulfate and methane (blue) and nitrate, methane plus sulfate (green). Relative gene expression levels were normalized against total 16S rRNA gene copies. The error bars depict the standard deviations in multiple measurements ($n = 3$).

expression in gene *mcrA*, which was in response to the highest AOM rate in Batch Test A-III (Fig. 5d).

Microscale levels of NO_3^-, NO_2^-, NH_4^+, SO_4^{2-} and S^{2-} in the biofilm were measured for the biotransformation of nitrogen and sulfur with methane feeding (Fig. 6). The highest nitrate concentration of 355.6 μM and highest sulfate concentration of 1014.8 μM were observed on the surface of the biofilm, and the nitrate concentration decreased hastily in the inner part of the biofilm compared with that in absence of sulfate (Fig. 6a and c), while the sulfate concentration decreased relaxedly compared with that in absence of nitrate (Fig. 6b and c). The interactions with both nitrate and sulfate as electron acceptors in biofilm resulted in a niche zone (at about depth of 500~850 μm) where nitrate was absent but sulfate is present for ANME-2d and SRB development (Fig. 6c).

3.4. Microscopic characterization of biofilm

At the end of the MBfR operation (Day 1200), biofilm samples were harvested from the hollow fibers and analyzed using FISH and SEM. We focused on ANME-2d and its potential symbiotic relationship with SRB in the presence of nitrate and sulfate. SRB interlaced around ANME-2d (Fig. 7a), and a widely distributed nanonet of flagellum-like structures overlaid the aggregations between ANME-2d and SRB (Fig. 7b). This nanonet resembles the nanowire connecting ANME-2d and SRB, but presented a non-linear, non-stacking network structure (Fig. 7c and f), with diameters of approximately 10~50 nm and apparent lengths of about 1500 nm or more (Fig. 7d and e). In contrast, the suspended culture of ANME-2d fed with nitrate and sulfate show smooth surfaces without any extracelluar appendages (Fig. S3), indicating that the observed intercellular structures are specific to consortial growth in biofilm and related to cellular attachment.

4. Discussion

4.1. Simultaneous nitrate- and sulfate-dependent AOM by ANME-2d

The nitrate reductase subunit harboring an active site (NarG) for nitrate reduction and a Rieske-cytochrome *b* complex for electron transport are encoded in the genome of ANME-2d clade (Arshad et al., 2015; Haroon et al., 2013), which permits the ANME-2d clade to perform nitrate-dependent AOM without any syntrophic partners (Welte et al., 2016). Previously known syntrophic partner for ANME-1 and -2a/b/c affiliated within SRB (*Desulfococcus* spp.) (Knittel and Boetius, 2009) was detected in our study based on the 16S rRNA gene amplicon sequence analysis, while only the clade of ANME-2d existed in the biofilm without any other known ANME lineages (Fig. 2 and S2). The results in our study suggested that AOM coupled to dissimilatory sulfate reduction was mediated by the ANME-2d clade in the syntrophic association with SRB partners. There is the genomic evidence suggesting that the subsurface ANME-2d clade, detected in groundwater environment, may

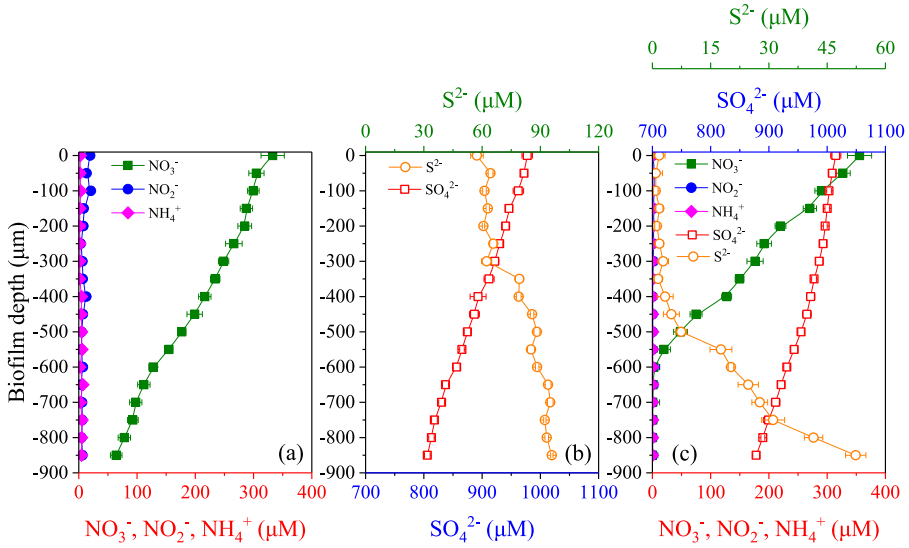

Fig. 6. Nitrogen and sulfur profiles in biofilm measured by microelectrode. (a) the profiles measured with nitrate as electron acceptor; (b) the profiles measured with sulfate as electron acceptor and (c) the profiles measured with both nitrate and sulfate as electron acceptor. The error bars depict the standard deviations in multiple measurements ($n = 3$).

directly couple AOM to sulfate reduction by using assimilatory sulfate reduction pathways (Ino et al., 2018). However, a dissimilatory role of sulfate reduction supported by the assimilatory genes in ANME lineages has not been shown (Yu et al., 2018).

The results of batch tests in our study confirmed that simultaneous reduction of nitrate and sulfate was associated with AOM, which suggested the ANME-2d clade not only carried out nitrate-dependent AOM, but also worked with SRB for converting sulfate to sulfide simultaneously. It is interesting that how sulfate-dependent AOM compete with nitrate-dependent AOM in the biofilm since the ANME-2d clade yields free energy change ($\Delta G^{0\prime}$) of -521 kJ mol^{-1} CH_4 for nitrate reduction (Eq. (2)), but the energy yield for sulfate reduction is as low as -21 kJ mol^{-1} CH_4 (Eq. (1)). Previous studies suggested that the observed low growth rate of ANME lineages for mediating sulfate-dependent AOM might be owing to the restricted energetics (Caldwell et al., 2008; Evans et al., 2019; McGlynn, 2017). However, even with the available energy and the apparent ability to utilize it, the ANME-2d clade performing nitrate-dependent AOM has been reported with a similar growth rate to sulfate-dependent AOM (Nauhaus et al., 2007; Nauhaus et al., 2005; Orphan et al., 2001a). Thus, the energy yield does not directly explain the lack of sulfate-dependent AOM activity in presence of methane, nitrate and sulfate in lab-reactors where the ANME-2d clade was dominated (Hu et al., 2009; Nie et al., 2019; Vaksmaa et al., 2017a). Based on the microelectrode measurements in our study, nitrate was consumed up soon in outer layers of biofilm (0–500 μm), while sulfate fully penetrated the biofilm and its reduction to sulfide mainly occurred inner layer (500–850 μm) (Fig. 6c). As a result, stratification of biofilms provided a niche zone for the ANME-2d clade and SRB where nitrate is absent but sulfate is present. Previous studies have speculated that the presence of sulfate enabled the ANME-2d clade to be active in nitrate-free lake sediments (Schubert et al., 2011; Su et al., 2019), in response to our findings that the absence of nitrate may provide an opportunity for the ANME-2d clade coupling with SRB for sulfate reduction. Thus, division of ANME archaea in anaerobic methane oxidation is not obligate and all clades of ANME organisms, including ANME-2d, could cooperate with SRB for sulfate-dependent AOM, which will have profound impacts for future microbiology research on anaerobic methane oxidation.

4.2. Putative mechanism of electron transfer between ANME-2d and SRB

Surface morphology of biofilm in our study showed novel nanonet structures connecting cells and expanding within the biofilm (Fig. 7b~f), which was speculated as conductive appendages involved in extracellular electron transfer in the syntrophy of ANME-2d clade and SRB. Previous study has demonstrated the direct interspecies electron transfer as principal mechanism for syntrophic coupling ANME-2b/c and SRB in consortia excluding the intermediates transfer between those two (McGlynn et al., 2015). In addition, there was other evidence for electron transfer between ANME-1, -2a, -3 and SRB, which showed the mechanism of extension ANME's redox-active surfaces beyond their cell envelope confines via forming nanowires similar with that in *Geobacter* and *Shewanella* spp. (Gao et al., 2017; McGlynn et al., 2015; Wegener et al., 2015). However, the observed nanonet structures in our work are distinct from pili-like structures, which are not a simple stack of nanowires. In general, the conductive protein appendages of the type-IV pili class form flexible filaments with one end anchored in the cell envelope and the other end connected extracellular biotic or abiotic electron acceptors for electron transfer (Craig et al., 2019; Shi et al., 2016).

Metatrascriptomic analysis in our study revealed significant up-regulation of gene *flaB* in ANME-2d for archaellum formation and gene *pilA* in SRB for pili formation during sulfate-dependent AOM (Fig. 4), which suggested that the unique nanonets were supposedly instructed by both pili and archaellum. The electrons from ANME-2d might travel along the nanonet to cells of SRB located on the nanonet where it could be consumed for sulfate reduction. Previous studies have shown that microbial cells can exchange electrons over centimeter distances through electrical connections (Lovley, 2017). Consequently, the activity of sulfate-dependent AOM would be independent of the distance between ANME-2d and SRB within biofilm. In fact, the archaellum from the other subtribe of ANME-2d clade has been suggested as conductive appendages for electron transfer during Mn(IV)-dependent AOM process (Leu-et al., 2020a). The archaellum from *Methanospirillum hungatei* archaea was capable of reducing extracellular electron acceptors, which was confirmed to be electrically conductive based on

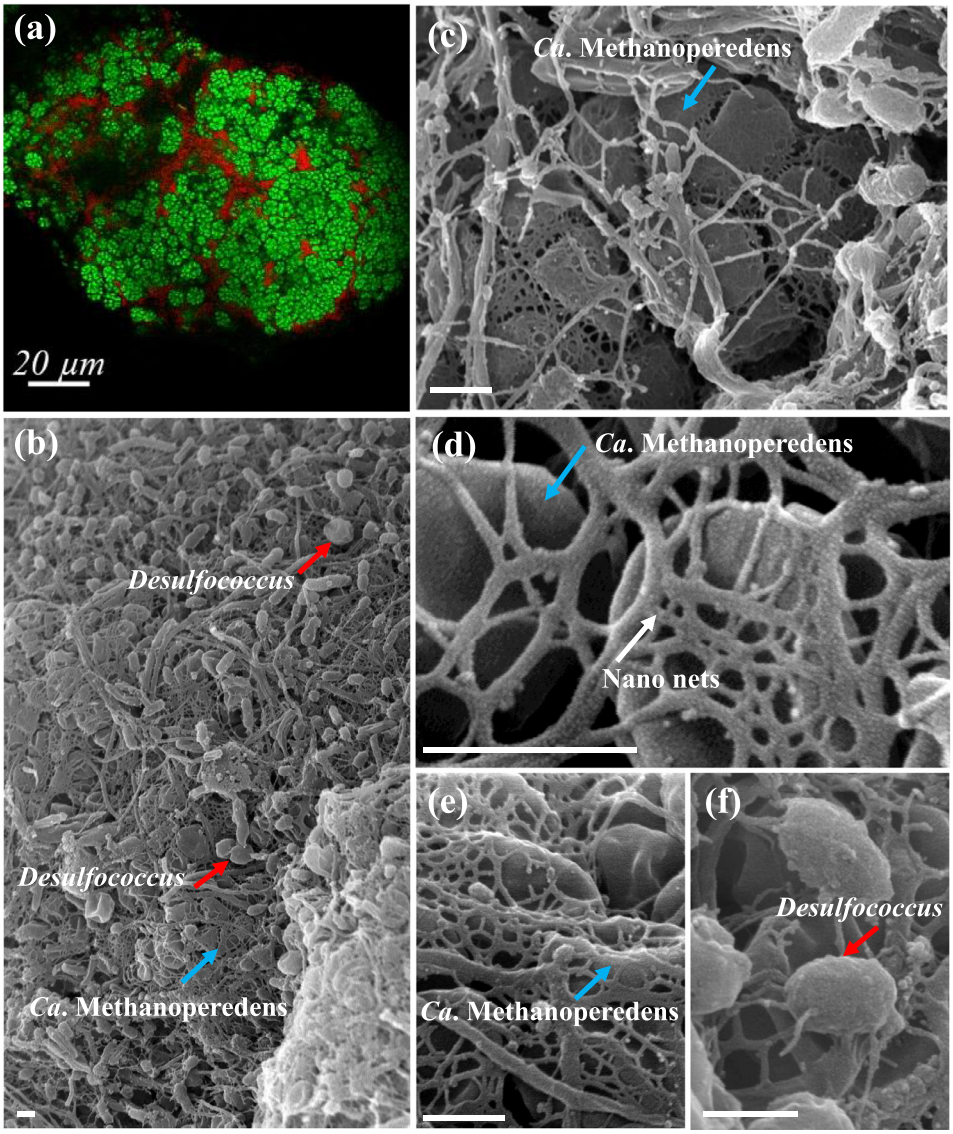

Fig. 7. Microscopic characterization of biofilm. (a) Representative FISH photomicrograph of *Candidatus* Methanoperedens (green) and *Desulfococcus* (red). Scale bar, 20 μm; (b-f) micrographs of SEM for visualization of structures attributed to interspecies electrons transfer between *Ca.* Methanoperedens (irregular cocci, 1.0–3.0 μm in diameter as sarcina-like clusters (Haroon et al., 2013)) and *Desulfococcus* (spherical to oval cells, 1.5–3.0 μm in diameter (Imhoff-Stuckle and Pfennig, 1983)). Scale bars, 500 nm. Nano nets of <50 nm diameter and up to several thousand nanometers in length connect both species.

the analysis of conductive atomic force microscopy (Walker et al., 2019).

In addition to the deductive conductive strictures, cytochrome *c* is proposed to be important for electron transfer between the ANME-2d and their syntrophic SRB partners. A large number of gene *cytC* encoding cytochrome c exist in the ANME-2d clade, and the expression of gene *cytC* in ANME-2d was significantly up-regulated with the development of SRB in our study. Cytochrome *c* reductase can act as electron storage in the cell membrane, which can overcome the physical and electrical barrier of cell envelop (Lai et al., 2020; Shi et al., 2016) for the cooperation of ANME-2d and SRB. Therefore, ANME-2d not only form partnership with NC10 bacteria and Anammox bacteria through chemical diffusion of nitrite and ammonium for nitrogen removal, but also might work with SRB through direct electron transfer via intercellular nanonet for sulfate reduction. As corollaries, the nanonets may serve as a matrix scaffold of biofilms to accommodate more cytochrome *c* with orderly arrangements, which might enhance the electron diffusion inside the biofilms, and the underlying bioelectrochemical characteristics of nanonet for direct electron transfer require further investigation.

4.3. AOM linking carbon, nitrogen and sulfur cycles

The microbial AOM plays a role in global methane regulation and reducing methane release from marine and freshwater ecosystems, which is well known to link the cycle of carbon and sulfur in marine (Fig. 8a) (Knittel and Boetius, 2009; McCalley, 2020; Smemo and Yavitt, 2011; Valentine, 2002) and carbon and nitrogen in freshwater (Fig. 8b) (Deutzmann and Schink, 2011; Deutzmann et al., 2014; Martinez-Cruz et al., 2018; Segarra et al., 2015). The results of our study show that AOM can link carbon, nitrogen and sulfur cycles in a biofilm reactor with counter-diffusional substrates (methane, nitrate and sulfate). In the reactor, methane as substrate diffuses through the membrane to biofilms while nitrate and sulfate as complementary substrates diffuse from bulk liquid into the biofilm, which is similar to the distribution of substances in the natural environments. Methane diffuses up-

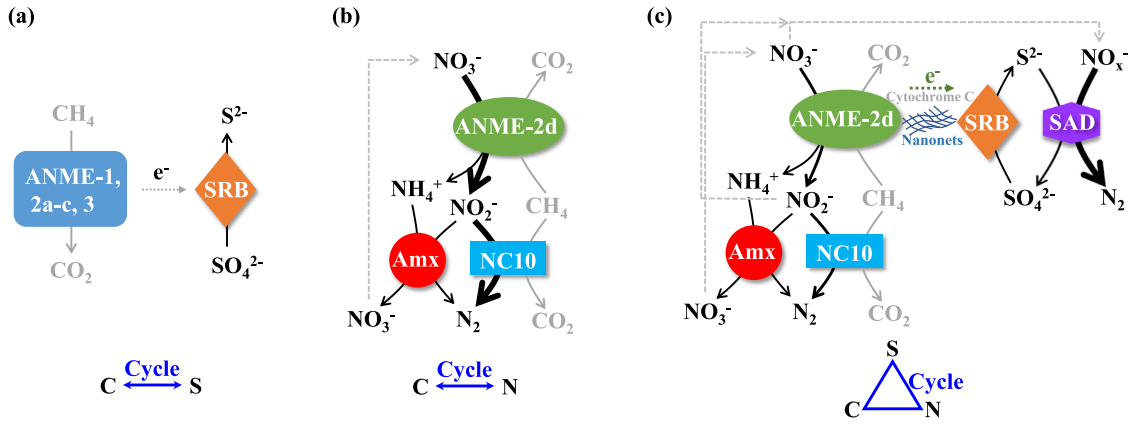

Fig. 8. A conceptual model for ANMEs interactions in marine system with sulfate as electron acceptor (a), in freshwater system with nitrate as electron acceptor (b) and in estuary or coastal zones with both sulfate and nitrate as electron acceptor (c).

wards from deeper sediments (Egger et al., 2018) while nitrate and sulfate with higher concentrations in overlaying water diffuse downwards (Burgin and Hamilton, 2007; Glombitza et al., 2016; Myrbo et al., 2017; Zhang et al., 2014). It is well established that the diffusion of those substances possibly provides suitable prerequisites for AOM linking carbon, nitrogen and sulfur cycles by the ANME-2d clade. The observed potential cycles involved with carbon, nitrogen and sulfur are shown in Fig. 8c. In the consortia for simultaneous nitrate- and sulfate-dependent AOM, the active NC10 and Anammox bacteria in the biofilm (Fig. S4a and b) reflected the syntrophic relationship between ANME-2d and other bacteria based on exchange of microbial metabolites. In addition, the active *Thiobacillus* spp. and *Sulfurovum* spp. (SAD) for sulfide oxidation with nitrate or nitrite as electron acceptor (Fig. S4c and d) confirmed the production of sulfide, which showed the syntrophy of ANME-2d and *Desulfococcus* spp. (SRB). The oxidation of sulfide with nitrate reduction not only avoided the accumulation of sulfide to inhibit the activity of AOM (Fig. S5), but also accelerated the formation of nitrate-deficient regions in the biofilm (Fig. 6). As microbial communities in natural environments predominantly existing as biofilms (Flemming et al., 2016; P. Stoodley et al., 2002), the dense cell aggregates coating mineral surfaces (Battin et al., 2003) in methane-, sulfate- and nitrate-rich sediments may control the carbon, sulfur and nitrogen cycles via simultaneous sulfate- and nitrate-dependent AOM process. Since nitrous oxide is a metabolic intermediate in the process of nitrate/nitrite reduction to dinitrogen gas by SAD (Lan et al., 2019; Liu et al., 2016b), the release of nitrous oxide in the simultaneous nitrate- and sulfate-dependent AOM process should be of further concern.

This work also suggested that the cooperation among the ANME-2d clade and other bacterial partners for simultaneous sulfate- and nitrate-dependent AOM process not only occurred at optimal temperature (30 °C) and room temperature (25 °C), but also occurred at the temperature close to that of the natural sediments (10 °C or 5 °C). Nevertheless, the microbial interactions presented here are susceptible to interference by other coexisting electron acceptors in the environments, such as iron, manganese, humus and so on (Bai et al., 2019; Ettwig et al., 2016). Still, the environments, such as nearshore sediments receiving reactive nitrogen compounds (Laverman et al., 2012) and freshwater environments with anthropogenic sulfate input (Chen et al., 2016; Lamers et al., 1998), possibly provide suitable prerequisites for simultaneous nitrate- and sulfate-dependent AOM by ANME-2d The link of carbon, nitrogen and sulfur cycles bonded by AOM could broad the implication to global methane cycle. In addition, nitrate-dependent AMO has been proposed to provide alternative solutions to simultaneously remove nitrogen and mitigate methane emission during wastewater treatment (Nie et al., 2020; Xie et al., 2017; Xie et al., 2018). However, sewage also contain considerable concentration of sulfate, resulting from application of sulfate coagulants during drinking water treatment and seawater toilet flushing (Zhang et al., 2019). The potential role of ANME-2d in carbon, nitrogen and sulfur cycles, and the contribution to methane and nitrogen turnover in natural environments and engineered wastewater treatment systems requires further investigation.

5. Conclusion

Overall, our findings provide a novel insight into AOM by ANME-2d clade which may link carbon, nitrogen and sulfur cycle occurring in estuary or coastal zone as the interface of marine and freshwater environments. Based on the bioreactor performance, reconstructed metabolic pathways and profiles of gene expression, this work shows that ANME-2d not only conduct nitrate reduction but also work with SRB for converting sulfate to sulfide. Gene *cytC* encoded by ANME-2d is found to be highly expressed during sulfate-dependent AOM suggesting cytochrome *c* plays an active role in electron transport form ANME-2d to SRB for sulfate reduction. Interestingly, unique nanonets connecting ANME-2d and SRB are observed in the biofilm, which are hypothesized as conductive appendages involved in extracellular electron transfer. In addition, our work also demonstrates that the produced sulfide can be oxidized back to sulfate by sulfide-oxidizing autotrophic denitrifier with nitrate or nitrite as electron acceptors, in turn alleviating sulfide accumulation and enhancing nitrogen removal. Meanwhile, future research should focus on confirming the conductivity of the unique nanonets similar to nanowires for electron transfer and the potential role of ANME-2d in carbon, nitrogen and sulfur cycles in natural environments and engineered wastewater treatment systems. Such the efforts will further expand our understanding of the ecological role of anaerobic methanotrophic archaea in natural environments.

Declaration of Competing Interest

The authors declare no financial, commercial, or personal conflict of interest involving the publication of this work.

We declare that we have no financial and personal relationships with other people or organizations that can inappropriately influence our work, there is no professional or other personal interest of any nature or kind in any product, service and/or company that could be construed as influencing the position presented in, or the review of, the manuscript entitled.

Acknowledgments

The authors would like to thank the Natural Science Foundation of China (Grant No. 51778173, 51808167 and 31870110), China Postdoctoral Science Foundation funded project (No. 2019T120276), Heilongjiang Postdoctoral Financial Assistance (No. LBH-Z17064), Postdoctoral Science Special Foundation of Heilongjiang (LBH-TZ11), Fundamental Research Funds for the Central Universities, Fok Ying Tung Education Foundation, State Key Laboratory of Urban Water Resource and Environment, Harbin Institute of Technology (2020DX15) and Shenzhen Science and Technology Innovation Project (KJYY20171011144235970) for supporting this study. Zhiguo Yuan is a recipient of the ARC Australian Laureate Fellowship (FL170100086).

Supplementary materials

Supplementary material associated with this article can be found, in the online version, at doi:10.1016/j.watres.2021.116928.

References

Arshad, A., Speth, D.R., de Graaf, R.M., Op den Camp, H.J.M., Jetten, M.S.M., Welte, C.U., 2015. A Metagenomics-based metabolic model of nitrate-dependent anaerobic oxidation of methane by methanoperedens-like archaea. Front. Microbiol. 6.

Bai, Y.-N., Wang, X.-N., Wu, J., Lu, Y.-Z., Fu, L., Zhang, F., Lau, T.-C., Zeng, R.J., 2019. Humic substances as electron acceptors for anaerobic oxidation of methane driven by ANME-2d. Water Res. 164, 114935 -114935.

Bankevich, A., Nurk, S., Antipov, D., Gurevich, A.A., Dvorkin, M., Kulikov, A.S., Lesin, V.M., Nikolenko, S.I., Pham, S., Prjibelski, A.D., 2012. SPAdes: a new genome assembly algorithm and its applications to single-cell sequencing. J. Comput. Biol. 19 (5), 455–477.

Battin, T.J., Kaplan, L.A., Denis Newbold, J., Hansen, C.M.E., 2003. Contributions of microbial biofilms to ecosystem processes in stream mesocosms. Nature 426 (6965), 439–442.

Bhattarai, S., Cassarini, C., Lens, P.N.L., 2019. Physiology and distribution of archaeal methanotrophs that couple anaerobic oxidation of methane with sulfate reduction.. Microbiol. Mol. Biol. Rev. 83.

Biddle, J.F., Cardman, Z., Mendlovitz, H., Albert, D.B., Lloyd, K.G., Boetius, A., Teske, A., 2012. Anaerobic oxidation of methane at different temperature regimes in Guaymas Basin hydrothermal sediments. ISME J. 6 (5), 1018–1031.

Boetius, A., Ravenschlag, K., Schubert, C.J., Rickert, D., Widdel, F., Gieseke, A., Amann, R., Jørgensen, B.B., Witte, U., Pfannkuche, O., 2000. A marine microbial consortium apparently mediating anaerobic oxidation of methane. Nature 407 (6804), 623–626.

Buchfink, B., Xie, C., Huson, D.H., 2015. Fast and sensitive protein alignment using DIAMOND. Nat. Methods 12 (1), 59–60.

Buhler, J.D., Lancaster, J.M., Jacob, A.C., Chamberlain, R.D., 2007. Mercury BLASTN: faster DNA sequence comparison using a streaming hardware architecture. In: Proc. of Reconfigurable Systems Summer Institute.

Burgin, A.J., Hamilton, S.K., 2007. Have we overemphasized the role of denitrification in aquatic ecosystems? A review of nitrate removal pathways. Front. Ecol. Environ. 5 (2), 89–96.

Caldwell, S.L., Laidler, J.R., Brewer, E.A., Eberly, J.O., Sandborgh, S.C., Colwell, F.S., 2008. Anaerobic oxidation of methane: mechanisms, bioenergetics, and the ecology of associated microorganisms. Environ. Sci. Technol. 42 (18), 6791–6799.

Cassarini, C., Zhang, Y. and Lens, P.N. (2018) Pressure sensitivity of ANME-3 predominant anaerobic methane oxidizing community from coastal marine Lake Grevelingen sediment. bioRxiv, 307082.

Chadwick, G.L., Jiménez Otero, F., Gralnick, J.A., Bond, D.R., Orphan, V.J., 2019. NanoSIMS imaging reveals metabolic stratification within current-producing biofilms. In: Proceedings of the National Academy of Sciences 201912498.

Chen, M., Li, X.-H., He, Y.-H., Song, N., Cai, H.-Y., Wang, C., Li, Y.-T., Chu, H.-Y., Krumholz, L.R., Jiang, H.-L., 2016. Increasing sulfate concentrations result in higher sulfide production and phosphorous mobilization in a shallow eutrophic freshwater lake. Water Res. 96, 94–104.

Clark, C.M., Simkin, S.M., Allen, E.B., Bowman, W.D., Belnap, J., Brooks, M.L., Collins, S.L., Geiser, L.H., Gilliam, F.S., Jovan, S.E., Pardo, L.H., Schulz, B.K., Stevens, C.J., Suding, K.N., Throop, H.L., Waller, D.M., 2019. Potential vulnerability of 348 herbaceous species to atmospheric deposition of nitrogen and sulfur in the United States. Nat. Plants 5 (7), 697–705.

Craig, L., Forest, K.T., Maier, B., 2019. Type IV pili: dynamics, biophysics and functional consequences. Nat. Rev. Microbiol. 17 (7), 429–440.

deBeer, D., Schramm, A., Santegoeds, C.M., Kuhl, M., 1997. A nitrite microsensor for profiling environmental biofilms. Appl. Environ. Microbiol. 63 (3), 973–977.

Deutzmann, J.S., 2020. Anaerobic Utilization of Hydrocarbons, Oils, and Lipids. Springer International Publishing, Cham, pp. 391–404 Boll, M. (ed), pp..

Deutzmann, J.S., Schink, B., 2011. Anaerobic oxidation of methane in sediments of lake constance, an oligotrophic freshwater lake. Appl. Environ. Microbiol. 77 (13), 4429–4436.

Deutzmann, J.S., Stief, P., Brandes, J., Schink, B., 2014. Anaerobic methane oxidation coupled to denitrification is the dominant methane sink in a deep lake. Proc. Natl. Acad. Sci. U. S. A. 111 (51), 18273–18278.

Egger, M., Riedinger, N., Mogollón, J.M., Jørgensen, B.B., 2018. Global diffusive fluxes of methane in marine sediments. Nat. Geosci. 11 (6), 421–425.

Engelbrektson, A., Kunin, V., Wrighton, K.C., Zvenigorodsky, N., Chen, F., Ochman, H., Hugenholtz, P., 2010. Experimental factors affecting PCR-based estimates of microbial species richness and evenness. ISME J. 4 (5), 642–647.

Ettwig, K.F., Shima, S., van de Pas-Schoonen, K.T., Kahnt, J., Medema, M.H., op den Camp, H.J.M., Jetten, M.S.M., Strous, M., 2008. Denitrifying bacteria anaerobically oxidize methane in the absence of Archaea. Environ. Microbiol. 10 (11), 3164–3173.

Ettwig, K.F., Zhu, B., Speth, D., Keltjens, J.T., Jetten, M.S.M., Kartal, B., 2016. Archaea catalyze iron-dependent anaerobic oxidation of methane. Proc. Natl. Acad. Sci. U. S. A. 113 (45), 12792–12796.

Evans, P.N., Boyd, J.A., Leu, A.O., Woodcroft, B., Parks, D.H., Hugenholtz, P., Tyson, G.W., 2019. An evolving view of methane metabolism in the Archaea. Nat. Rev. Microbiol. 17 (4), 219–232.

Ferguson, G., Gleeson, T., 2012. Vulnerability of coastal aquifers to groundwater use and climate change. Nat. Clim. Chang. 2 (5), 342–345.

Flemming, H.-C., Wingender, J., Szewzyk, U., Steinberg, P., Rice, S.A., Kjelleberg, S., 2016. Biofilms: an emergent form of bacterial life. Nat. Rev. Microbiol. 14 (9), 563–575.

Fletcher, S.E.M., Schaefer, H., 2019. Rising methane: a new climate challenge. Science 364 (6444), 932–933.

Gambelli, L., Guerrero-Cruz, S., Mesman, R.J., Cremers, G., Jetten, M.S.M., Op den Camp, H.J.M., Kartal, B., Lueke, C., van Niftrik, L., 2018. Community composition and ultrastructure of a nitrate-dependent anaerobic methane-oxidizing enrichment culture. Appl. Environ. Microbiol. 84 (3), e02186 -02117.

Gao, Y., Lee, J., Neufeld, J.D., Park, J., Rittmann, B.E., Lee, H.-S., 2017. Anaerobic oxidation of methane coupled with extracellular electron transfer to electrodes. Sci. Rep. 7 (1), 5099.

Glöckner, F.O., Amann, R., Alfreider, A., Pernthaler, J., Psenner, R., Trebesius, K., Schleifer, K.-H., 1996. An in situ hybridization protocol for detection and identification of planktonic bacteria. Syst. Appl. Microbiol. 19 (3), 403–406.

Glombitza, C., Adhikari, R.R., Riedinger, N., Gilhooly III, W.P., Hinrichs, K.-U., Inagaki, F., 2016. Microbial sulfate reduction potential in coal-bearing sediments down to similar to 2.5km below the seafloor off Shimokita Peninsula, Japan.. Front. Microbiol. 7.

Gudasz, C., Bastviken, D., Steger, K., Premke, K., Sobek, S., Tranvik, L.J., 2010. Temperature-controlled organic carbon mineralization in lake sediments. Nature 466 (7305), 478–481.

Haroon, M.F., Hu, S., Shi, Y., Imelfort, M., Keller, J., Hugenholtz, P., Yuan, Z., Tyson, G.W., 2013. Anaerobic oxidation of methane coupled to nitrate reduction in a novel archaeal lineage. Nature 500 (7464), 567–570.

Holler, T., Widdel, F., Knittel, K., Amann, R., Kellermann, M.Y., Hinrichs, K.-U., Teske, A., Boetius, A., Wegener, G., 2011. Thermophilic anaerobic oxidation of methane by marine microbial consortia. ISME J. 5 (12), 1946–1956.

Hu, S., Zeng, R.J., Burow, L.C., Lant, P., Keller, J., Yuan, Z., 2009. Enrichment of denitrifying anaerobic methane oxidizing microorganisms. Environ. Microbiol. Rep. 1 (5), 377–384.

Hua, Z.-S., Han, Y.-J., Chen, L.-X., Liu, J., Hu, M., Li, S.-J., Kuang, J.-L., Chain, P.S.G., Huang, L.-N., Shu, W.-S., 2015. Ecological roles of dominant and rare prokaryotes in acid mine drainage revealed by metagenomics and metatranscriptomics. ISME J. 9 (6), 1280–1294.

Imhoff-Stuckle, D., Pfennig, N., 1983. Isolation and characterization of a nicotinic acid-degrading sulfate-reducing bacterium, Desulfococcus niacini sp. nov. Arch. Microbiol. 136 (3), 194–198.

Ino, K., Hernsdorf, A.W., Konno, U., Kouduka, M., Yanagawa, K., Kato, S., Sunamura, M., Hirota, A., Togo, Y.S., Ito, K., Fukuda, A., Iwatsuki, T., Mizuno, T., Komatsu, D.D., Tsunogai, U., Ishimura, T., Amano, Y., Thomas, B.C., Banfield, J.F., Suzuki, Y., 2018. Ecological and genomic profiling of anaerobic methane-oxidizing archaea in a deep granitic environment. Isme J. 12 (1), 31–47.

Jiang, G., Sharma, K.R., Guisasola, A., Keller, J., Yuan, Z., 2009. Sulfur transformation in rising main sewers receiving nitrate dosage. Water Res. 43 (17), 4430–4440.

Joshi, N. and Sickle, F. (2011) Sickle: a sliding-window, adaptive, quality-based trimming tool for FastQ files.

Kang, D.D., Froula, J., Egan, R., Wang, Z., 2015. MetaBAT, an efficient tool for accurately reconstructing single genomes from complex microbial communities. PeerJ 3, e1165.

Kapoor, V., Li, X., Elk, M., Chandran, K., Impellitteri, C.A., Santo Domingo, J.W., 2015. Impact of heavy metals on transcriptional and physiological activity of nitrifying bacteria. Environ. Sci. Technol. 49 (22), 13454–13462.

Khanal, S.K., Huang, J.-C., 2003. ORP-based oxygenation for sulfide control in anaerobic treatment of high-sulfate wastewater. Water Res. 37 (9), 2053–2062.

Knittel, K., Boetius, A., 2009. Anaerobic oxidation of methane: progress with an unknown process. Annu. Rev. Microbiol. 63, 311–334.

Lagesen, K., Hallin, P., Rødland, E.A., Stærfeldt, H.-H., Rognes, T., Ussery, D.W., 2007. RNAmmer: consistent and rapid annotation of ribosomal RNA genes. Nucleic Acids Res. 35 (9), 3100–3108.

Lai, B., Bernhardt, P.V., Krömer, J.O., 2020. Cytochrome c reductase is a key enzyme involved in the extracellular electron transfer pathway towards transition metal complexes in Pseudomonas Putida. ChemSusChem 13, 5308–5317.

Lamers, L.P.M., Tomassen, H.B.M., Roelofs, J.G.M., 1998. Sulfate-induced eutrophication and phytotoxicity in freshwater wetlands. Environ. Sci. Technol. 32 (2), 199–205.
Lan, L., Zhao, J., Wang, S., Li, X., Qiu, L., Liu, S., Bin Nasry, A.A.N., 2019. NO and N2O accumulation during nitrite-based sulfide-oxidizing autotrophic denitrification. Bioresour. Technol. Rep. 7, 100190.
Laverman, A.M., Pallud, C., Abell, J., Cappellen, P.V., 2012. Comparative survey of potential nitrate and sulfate reduction rates in aquatic sediments. Geochim. Cosmochim. Acta 77, 474–488.
Leu, A.O., Cai, C., McIlroy, S.J., Southam, G., Orphan, V.J., Yuan, Z., Hu, S., Tyson, G.W., 2020a. Anaerobic methane oxidation coupled to manganese reduction by members of the Methanoperedenaceae. ISME J. 14, 1030–1041.
Leu, A.O., McIlroy, S.J., Ye, J., Parks, D.H., Orphan, V.J., Tyson, G.W., 2020b. Lateral gene transfer drives metabolic flexibility in the anaerobic methane-oxidizing archaeal family methanoperedenaceae. MBio 11 (3), e01325 -01320.
Liu, C., Han, K., Lee, D.J., Wang, Q., 2016a. Simultaneous biological removal of phenol, sulfide, and nitrate using expanded granular sludge bed reactor. Appl. Microbiol. Biotechnol. 100 (9), 4211–4217.
Liu, H., Liu, X., Ding, N., 2020. An innovative in situ monitoring of sulfate reduction within a wastewater biofilm by H2S and SO42− microsensors. Int. J. Environ. Res. Public Health 17 (6), 2023.
Liu, Y., Peng, L., Ngo, H.H., Guo, W., Wang, D., Pan, Y., Sun, J., Ni, B.-J., 2016b. Evaluation of nitrous oxide emission from sulfide- and sulfur-based autotrophic denitrification processes. Environ. Sci. Technol. 50 (17), 9407–9415.
Lloyd, K.G., Alperin, M.J., Teske, A., 2011. Environmental evidence for net methane production and oxidation in putative ANaerobic MEthanotrophic (ANME) archaea. Environ. Microbiol. 13 (9), 2548–2564.
Lovley, D.R., 2017. Happy together: microbial communities that hook up to swap electrons. Isme J. 11 (2), 327–336.
Martinez-Cruz, K., Sepulveda-Jauregui, A., Casper, P., Anthony, K.W., Smemo, K.A., Thalasso, F., 2018. Ubiquitous and significant anaerobic oxidation of methane in freshwater lake sediments. Water Res. 144, 332–340.
McCalley, C.K., 2020. Methane-eating microbes. Nat. Clim. Chang. 10 (4), 275–276.
McGlynn, S.E., 2017. Energy metabolism during anaerobic methane oxidation in ANME archaea. Microbes Environ. 32 (1), 5–13.
McGlynn, S.E., Chadwick, G.L., Kempes, C.P., Orphan, V.J., 2015. Single cell activity reveals direct electron transfer in methanotrophic consortia. Nature 526 (7574), 531–535.
Michaelis, W., Seifert, R., Nauhaus, K., Treude, T., Thiel, V., Blumenberg, M., Knittel, K., Gieseke, A., Peterknecht, K., Pape, T., Boetius, A., Amann, R., Jorgensen, B.B., Widdel, F., Peckmann, J., Pimenov, N.V., Gulin, M.B., 2002. Microbial reefs in the Black Sea fueled by anaerobic oxidation of methane. Science 297 (5583), 1013–1015.
Milucka, J., Ferdelman, T.G., Polerecky, L., Franzke, D., Wegener, G., Schmid, M., Lieberwirth, I., Wagner, M., Widdel, F., Kuypers, M.M.M., 2012. Zero-valent sulphur is a key intermediate in marine methane oxidation. Nature 491 (7425) 541–+.
Miner, G., 2006. Standard methods for the examination of water and wastewater. 21st Edition. J. Am. Water Works Assoc. (1) 130.
Moraes, B.S., Souza, T.S.O., Foresti, E., 2011. Characterization and kinetics of sulfide-oxidizing autotrophic denitrification in batch reactors containing suspended and immobilized cells. Water Sci. Technol. 64 (3), 731–738.
Moriya, Y., Itoh, M., Okuda, S., Yoshizawa, A.C., Kanehisa, M., 2007. KAAS: an automatic genome annotation and pathway reconstruction server. Nucleic Acids Res. 35 (suppl_2), W182–W185.
Myrbo, A., Swain, E.B., Engstrom, D.R., Coleman Wasik, J., Brenner, J., Dykhuizen Shore, M., Peters, E.B., Blaha, G., 2017. Sulfide generated by sulfate reduction is a primary controller of the occurrence of wild rice (Zizania palustris) in shallow aquatic ecosystems. J. Geophys. Res. 122 (11), 2736–2753.
Nauhaus, K., Albrecht, M., Elvert, M., Boetius, A., Widdel, F., 2007. In vitro cell growth of marine archaeal-bacterial consortia during anaerobic oxidation of methane with sulfate. Environ. Microbiol. 9 (1), 187–196.
Nauhaus, K., Treude, T., Boetius, A., Krüger, M., Nauhaus, K., Treude, T., Boetius, A., Kruger, M., 2005. Environmental regulation of the anaerobic oxidation of methane: a comparison of ANME-I and ANME-II communities. Environ. Microbiol. 7, 98–106 Environ. Microbiol. 7, 98-106.
Nie, W.-B., Ding, J., Xie, G.-J., Yang, L., Peng, L., Tan, X., Liu, B.-F., Xing, D.-F., Yuan, Z., Ren, N.-Q., 2021. Anaerobic oxidation of methane coupled with dissimilatory nitrate reduction to ammonium fuels anaerobic ammonium oxidation. Environ. Sci. Technol. 55 (2), 1197–1208.
Nie, W.-B., Xie, G.-J., Ding, J., Lu, Y., Liu, B.-F., Xing, D.-F., Wang, Q., Han, H.-J., Yuan, Z., Ren, N.-Q., 2019. High performance nitrogen removal through integrating denitrifying anaerobic methane oxidation and Anammox: from enrichment to application. Environ. Int. 132, 105107.
Nie, W.-B., Xie, G.-J., Ding, J., Peng, L., Lu, Y., Tan, X., Yue, H., Liu, B.-F., Xing, D.-F., Meng, J., Han, H.-J., Ren, N.-Q., 2020. Operation strategies of n-DAMO and Anammox process based on microbial interactions for high rate nitrogen removal from landfill leachate. Environ. Int. 139, 105596.
Orphan, V., House, C., Hinrichs, K.-U., McKeegan, K., DeLong, E., 2001a. Methane–consuming Archaea revealed by directly coupled isotopic and phylogenetic analysis. Science 293, 484–487.
Orphan, V.J., Hinrichs, K.-U., Ussler, W., Paull, C.K., Taylor, L.T., Sylva, S.P., Hayes, J.M., Delong, E.F., 2001b. Comparative analysis of methane-oxidizing archaea and sulfate-reducing bacteria in anoxic marine sediments. Appl. Environ. Microbiol. 67 (4), 1922–1934.
Orphan, V.J., House, C.H., Hinrichs, K.U., McKeegan, K.D., DeLong, E.F., 2002. Multiple archaeal groups mediate methane oxidation in anoxic cold seep sediments. Proc. Natl. Acad. Sci. U. S. A. 99 (11), 7663–7668.
Pachauri, R.K., Allen, M.R., Barros, V.R., Broome, J., Cramer, W., Christ, R., Church, J.A., Clarke, L., Dahe, Q., Dasgupta, P., 2014. Climate change 2014: synthesis report. Contribution of Working Groups I, II and III to the fifth assessment report of the Intergovernmental Panel on Climate Change. Ipcc.
Parks, D.H., Imelfort, M., Skennerton, C.T., Hugenholtz, P., Tyson, G.W., 2015. CheckM: assessing the quality of microbial genomes recovered from isolates, single cells, and metagenomes. Genome Res. 25 (7), 1043–1055.
Pasquali, C.E.L., Hernando, P.F., Alegría, J.S.D., 2007. Spectrophotometric simultaneous determination of nitrite, nitrate and ammonium in soils by flow injection analysis. Anal. Chim. Acta 600 (1–2), 177–182.
Raghoebarsing, A.A., Pol, A., van de Pas-Schoonen, K.T., Smolders, A.J.P., Ettwig, K.F., Rijpstra, W.I.C., Schouten, S., Damste, J.S.S., Op den Camp, H.J.M., Jetten, M.S.M., Strous, M., 2006. A microbial consortium couples anaerobic methane oxidation to denitrification. Nature 440 (7086), 918–921.
Scheller, S., Yu, H., Chadwick, G.L., McGlynn, S.E., Orphan, V.J., 2016. Artificial electron acceptors decouple archaeal methane oxidation from sulfate reduction. Science 351 (6274), 703–707.
Schubert, C.J., Vazquez, F., Lösekann-Behrens, T., Knittel, K., Tonolla, M., Boetius, A., 2011. Evidence for anaerobic oxidation of methane in sediments of a freshwater system (Lago di Cadagno). FEMS Microbiol. Ecol. 76 (1), 26–38.
Segarra, K.E.A., Schubotz, F., Samarkin, V., Yoshinaga, M.Y., Hinrichs, K.U., Joye, S.B., 2015. High rates of anaerobic methane oxidation in freshwater wetlands reduce potential atmospheric methane emissions. Nat. Commun. 6 (1), 7477.
Shen, L.-d., Ouyang, L., Zhu, Y., Trimmer, M., 2019. Active pathways of anaerobic methane oxidation across contrasting riverbeds. ISME J. 13 (3), 752–766.
Shen, L.-d., Wu, H.-s., Liu, X., Li, J., 2017. Cooccurrence and potential role of nitrite- and nitrate-dependent methanotrophs in freshwater marsh sediments. Water Res. 123, 162–172.
Shi, L., Dong, H., Reguera, G., Beyenal, H., Lu, A., Liu, J., Yu, H.-Q., Fredrickson, J.K., 2016. Extracellular electron transfer mechanisms between microorganisms and minerals. Nat. Rev. Microbiol. 14 (10), 651–662.
Smemo, K.A., Yavitt, J.B., 2011. Anaerobic oxidation of methane: an underappreciated aspect of methane cycling in peatland ecosystems? Biogeosciences 8 (3), 779–793.
Stoodley, P., Sauer, K., Davies, D.G., Costerton, J.W., 2002. Biofilms as complex differentiated communities. Annu. Rev. Microbiol. 56 (1), 187–209.
Su, G.Y., Zopfi, J., Yao, H.Y., Steinle, L., Niemann, H., Lehmann, M.F., 2019. Manganese/iron-supported sulfate-dependent anaerobic oxidation of methane by archaea in lake sediments. Limnol. Oceanogr. 65 (2020), 863–875.
Szynkiewicz, A., Witcher, J.C., Modelska, M., Borrok, D.M., Pratt, L.M., 2011. Anthropogenic sulfate loads in the Rio Grande, New Mexico (USA). Chem. Geol. 283 (3), 194–209.
Tan, S., Liu, J., Fang, Y., Hedlund, B.P., Lian, Z.-H., Huang, L.-Y., Li, J.-T., Huang, L.-N., Li, W.-J., Jiang, H.-C., 2019. Insights into ecological role of a new deltaproteobacterial order Candidatus Acidulodesulfobacterales by metagenomics and metatranscriptomics. ISME J. 13 (8), 2044–2057.
Timmers, P.H.A., Welte, C.U., Koehorst, J.J., Plugge, C.M., Jetten, M.S.M., Stams, A.J.M., 2017. Reverse methanogenesis and respiration in methanotrophic archaea. Archaea 2017, 1654237.
Vaksmaa, A., Guerrero-Cruz, S., van Alen, T.A., Cremers, G., Ettwig, K.F., Luke, C., Jetten, M.S.M., 2017a. Enrichment of anaerobic nitrate-dependent methanotrophic 'Candidatus Methanoperedens nitroreducens' archaea from an Italian paddy field soil. Appl. Microbiol. Biotechnol. 101 (18), 7075–7084.
Vaksmaa, A., van Alen, T.A., Ettwig, K.F., Lupotto, E., Valè, G., Jetten, M.S.M., Lüke, C., 2017b. Stratification of diversity and activity of methanogenic and methanotrophic microorganisms in a nitrogen-fertilized Italian paddy soil. Front. Microbiol. 8 (2127).
Valentine, D.L., 2002. Biogeochemistry and microbial ecology of methane oxidation in anoxic environments: a review. Antonie Van Leeuwenhoek Int. J. Gen. Mol. Microbiol. 81 (1–4), 271–282.
Walker, D.J.F., Martz, E., Holmes, D.E., Zhou, Z., Nonnenmann, S.S., Lovley, D.R., 2019. The archaellum of Methanospirillum hungatei is electrically conductive. MBio 10 (2), e00579 -00519.
Wang, F.-P., Zhang, Y., Chen, Y., He, Y., Qi, J., Hinrichs, K.-U., Zhang, X.-X., Xiao, X., Boon, N., 2014. Methanotrophic archaea possessing diverging methane-oxidizing and electron-transporting pathways. ISME J. 8 (5), 1069–1078.
Wegener, G., Krukenberg, V., Riedel, D., Tegetmeyer, H.E., Boetius, A., 2015. Intercellular wiring enables electron transfer between methanotrophic archaea and bacteria. Nature 526 (7574), 587–590.
Welte, C.U., Rasigraf, O., Vaksmaa, A., Versantvoort, W., Arshad, A., Op den Camp, H.J.M., Jetten, M.S.M., Luke, C., Reimann, J., 2016. Nitrate- and nitrite-dependent anaerobic oxidation of methane. Environ. Microbiol. Rep. 8 (6), 941–955.
Xie, G.-J., Cai, C., Hu, S., Yuan, Z., 2017. Complete nitrogen removal from synthetic anaerobic sludge digestion liquor through integrating Anammox and denitrifying anaerobic methane oxidation in a membrane biofilm reactor. Environ. Sci. Technol. 51 (2), 819–827.
Xie, G.-J., Liu, T., Cai, C., Hu, S., Yuan, Z., 2018. Achieving high-level nitrogen removal in mainstream by coupling anammox with denitrifying anaerobic methane oxidation in a membrane biofilm reactor. Water Res. 131, 196–204.
Yu, H., Susanti, D., McGlynn, S.E., Skennerton, C.T., Chourey, K., Iyer, R., Scheller, S., Tavormina, P.L., Hettich, R.L., Mukhopadhyay, B., Orphan, V.J., 2018. Comparative

genomics and proteomic analysis of assimilatory sulfate reduction pathways in anaerobic methanotrophic archaea. Front. Microbiol. 9.
Zhang, L., Wang, S., Wu, Z., 2014. Coupling effect of pH and dissolved oxygen in water column on nitrogen release at water-sediment interface of Erhai Lake, China. Estuarine Coast. Shelf Sci. 149, 178–186.
Zhang, Y., Hua, Z.-S., Lu, H., Oehmen, A., Guo, J., 2019. Elucidating functional microorganisms and metabolic mechanisms in a novel engineered ecosystem integrating C, N, P and S biotransformation by metagenomics. Water Res. 148, 219–230.